Atmos. Chem. Phys. Discuss., 10, 19811–19844, 2010
www.atmos-chem-phys-discuss.net/10/19811/2010/
doi:10.5194/acpd-10-19811-2010

Atmospheric Chemistry and Physics Discussions

An extended secondary organic aerosol formation model: effect of oxidation aging and implications

F. Yu

Atmospheric Sciences Research Center, State University of New York, Albany, New York, USA

Received: 25 July 2010 – Accepted: 13 August 2010 – Published: 23 August 2010

Correspondence to: F. Yu (yfq@asrc.cestm.albany.edu)

Published by Copernicus Publications on behalf of the European Geosciences Union.

Abstract

The widely used 2-product secondary organic aerosol (SOA) formation model has been extended in this study to consider the volatility changes of secondary organic gases (SOGs) arising from the aging process. In addition to semi-volatile SOG (SV-SOG) and medium-volatile SOG (MV-SOG), we add a third component representing low-volatile SOG (LV-SOG) and design a scheme to transfer MV-SOG to SV-SOG and SV-SOG to LV-SOG associated with oxidation aging. This extended SOA formation model has been implemented in a global aerosol model (GEOS-Chem) and the co-condensation of H_2SO_4 and LV-SOG on pre-existing particles is explicitly simulated. We show that, over many parts of the continents, LV-SOG concentrations are generally a factor of ~2–20 higher than those of H_2SO_4 and LV-SOG condensation significantly enhances particle growth rates. Comparisons of the simulated and observed evolution of particle size distributions in a boreal forest site (Hyytiälä, Finland) clearly show that LV-SOG condensation is critical in order to bring the simulations closer to the observations. With the new SOA formation scheme, annual mean SOA mass increases by a fact of 2–10 in many parts of the boundary layer and reaches above 1 $\mu g\,m^{-3}$ in most parts of the main continents. As a result of enhanced surface area and reduced nucleation rates, the new scheme generally decreases the concentration of condensation nuclei larger than 10 nm (CN10) by 3–30% in the lower boundary layer, which slightly improves agreement between simulated annual mean CN10 values and those observed in 21 surface sites around the globe. SOG oxidation aging and LV-SOG condensation substantially increases the concentration of cloud condensation nuclei at a water supersaturation ratio of 0.2%, ranging from ~3–10% over a large fraction of oceans to ~10–100% over major continents. Our study highlights the importance for global aerosol models to explicitly account for the oxidation aging of SOGs and their contribution of particle growth.

ACPD
10, 19811–19844, 2010

1 Introduction

Particles in the atmosphere have important impacts on regional to global climate, air quality, and human health. The significance of these impacts depends strongly on the particle properties including concentration, size, composition, hygroscopic parameter, and mixing state. One major uncertainty in present regional and global aerosol simulations is associated with the contribution of secondary organic aerosol (SOA) to particle growth, size, and mass. Formation and the subsequent growth of secondary particles observed frequently in various parts of the globe (Kulmala et al., 2004; Yu et al., 2008) are an important source of atmospheric aerosols. While the involvement of H_2SO_4 in atmospheric particle formation is well established, many field measurements indicate that the growth rates of nucleated particles are commonly a factor of ~2–20 higher than can be explained by the H_2SO_4 vapor condensation alone (e.g., Kuang et al., 2010). The condensation of low volatile organic species, which is poorly represented in current aerosol models, is likely to dominate the growth rate of freshly nucleated particles in many regions. Particle composition measurements indicate that organic aerosol (OA) makes up ~20–90% of submicron particulate mass (Zhang et al., 2007) and SOA accounts for a large fraction (~72±21%) of these OA mass at many locations around the globe (Jimenez et al., 2009). Atmospheric chemical transport models have been known to underestimate atmospheric OA and SOA mass, in some cases by a factor of 10 or more (Heald et al., 2005; Volkamer et al., 2006). In addition to uncertainties in the emission inventories of SOA precursors and laboratory data of SOA yielding, the poor representation of SOA formation in the models could also lead to model under-prediction.

The chemical and physical processes associated with SOA formation are very complex (Kroll and Seinfeld, 2008; Hallquist et al., 2009) because of the large amount of different organic compounds involved. Present model predictions of atmospheric SOA formation are largely built upon the theoretical foundations on organic gas/particle partitioning developed by Pankow in the 1990s (Pankow, 1994) and extended by Odum

ACPD
10, 19811–19844, 2010

et al. to SOA formation (Odum et al., 1996). According to the theory, partitioning of each semi-volatile compound m between secondary organic gas (SOG_m) and aerosol (SOA_m) phase can be described by an equilibrium partitioning coefficient $K_{p,m}$ ($m^3\,\mu g^{-1}$), or equivalently (Donahue et al., 2006) its inverse, the effective saturation vapor concentration, C_m^* ($\mu g\,m^{-3}$),

$$\frac{C_{SOA_m}}{C_{SOG_m}} = K_{p,m} M_{absorb} = \frac{M_{absorb}}{C_m^*} \quad (1)$$

where C_{SOA_m} and C_{SOG_m} are the mass concentration ($\mu g\,m^{-3}$) of specie m in the aerosol and gas phases, respectively. M_{absorb} is the mass concentration ($\mu g\,m^{-3}$) of the total absorbing particle phase and refers only to the particulate matter participating in absorptive partitioning.

If the oxidation of a hydrocarbon (HC) leads to n semi-volatile products, Odum et al. (1996) showed that the SOA yield Y, defined as the mass of SOA produced (ΔM_{OA}) per unit mass of hydrocarbon oxidized (ΔM_{HC}), can be derived from Eq. (1) and expressed as:

$$Y = \frac{\Delta M_{OA}}{\Delta M_{HC}} = \sum_{k=1}^{n} \frac{\alpha_k K_{p,k} M_{absorb}}{1 + K_{p,k} M_{absorb}} = \sum_{k=1}^{n} \frac{\alpha_k}{1 + C_k^* / M_{absorb}} \quad (2)$$

where α_k is the mass-based stoichiometric yield of product k, and n is total number of products.

Because of the large number of products formed in a given HC oxidation reaction and the difficulty in measuring individual semi-volatile compounds, two surrogate products (i.e., n=2) have been widely used to express the volatility distribution of the oxidation products (Odum et al., 1996) and are considered as the standard means of representing laboratory SOA yield data in many experimental studies (Seinfeld and Pankow, 2003). The 2-product (i.e., n=2) version of Eq. (2), or 2-product model of SOA formation, has been employed in a number of regional and global models such as CMAQ

ACPD
10, 19811–19844, 2010

(Schell et al., 2001), CMAQ-MADRID (Zhang et al., 2004), GEOS-Chem (Chung and Seinfeld, 2002; Liao et al., 2007); GISS GCM II-prime (Chung and Seinfeld, 2002), and TM-3 with CBM-4 (Tsigaridis and Kanakidou, 2003).

It should be noted that the above described 2-product SOA formation model has been derived based on laboratory measurements which generally last for several hours. As a result, the 2-product SOA formation model does not take into account the SOG aging process which has been observed in the atmosphere and in the laboratory for the time beyond several hours of reactions (Donahue et al., 2006; Rudich et al., 2007; Kroll and Seinfeld, 2008; Hallquist et al., 2009; Jimenez et al., 2009). It has been found in these recent investigations that OA and OA precursor gases become increasingly oxidized, less volatile, and more hygroscopic as a result of continuous aging in the atmosphere (e.g., Jimenez et al., 2009). Kroll and Seinfeld (2008) pointed out that, in order to gain a quantitative and predictive understanding of SOA formation, the volatility changes arising from the aging process must be parameterized and included in models.

The traditional equilibrium partitioning-based 2-product model does not model the kinetic growth of particles by condensation, which is a kinetic rather than an equilibrium process. As mentioned earlier, field measurements indicate that the growth rates of nucleated particles are commonly a factor of ~2–20 higher than can be explained by the H_2SO_4 vapor condensation alone, likely a result of SOA condensation (e.g., Kuang et al., 2010). Since the particle growth rates are essential to properly account for the contribution of nucleated particles to CCN and thus accurately predict the CCN concentrations, it is critical to understand the spatial-temporal variations of the concentrations of condensable SOGs and properly represent their contribution to secondary particle growth in the aerosol models. In addition, to explicitly resolve the growth of nucleated particles through the condensation (not partitioning) of aged SOGs is important in the sense that the condensation of low-volatile SOGs can enable additional more volatile organics to be uptaken through partitioning which further grow the secondary particles.

ACPD
10, 19811–19844, 2010

The main objectives of this study are to extend the 2-product SOA formation model to aging and to represent the kinetic condensation of low-volatile SOGs on atmospheric particles in a global aerosol model. The scheme to consider the aging process as well as predict the concentration of condensable low-volatile SOGs is described in Sect. 2. The extended 2-product SOA formation has been implemented within the GEOS-Chem framework and the effects of the oxidation aging on simulated particle properties are presented in Sect. 3. Section 4 is the summary and discussion.

2 Extended SOA formation model

In GEOS-Chem v8-2-3 on which this study is based, reactive biogenic volatile organic compounds (VOCs) are grouped into six categories (VOC_i, i=1–6), with VOC_1=α-pinene+β-pinene+sabinene+careen+terpenoid ketones; VOC_2=limonene; VOC_3=α-terpinene+γ-terpinene+terpinolene; VOC_4=myrcene+terpenoid alcohols+ocimene; VOC_5=sesquiterpenes; and VOC_6=isoprene. Grouping is based on rate constants and aerosol yield parameters determined from laboratory chamber studies (Griffin et al., 1999; Seinfeld and Pankow, 2003; Henze and Seinfeld, 2006), and schemes used to represent SOA formation from the oxidation of these VOCs have been described in Chung and Seinfeld (2002) and Liao et al. (2007). For each of the first four VOC categories (VOC_{1-4}), there are three oxidation products, two for combined O_3 and OH oxidation and one for NO_3 oxidation. There are only two products for sesquiterpenes (i.e., VOC_5: one for combined O_3 and OH oxidation and one for NO_3 oxidation) and for isoprene (i.e., VOC_6: two for combined O_3 and OH oxidation and no NO_3 oxidation). In brief, the oxidation reactions of VOC_i with O_3+OH (OX_1) and NO_3 (OX_2) produce 16 groups of SOGs which then lead to the formation of 16 groups of SOAs through equilibrium partitioning (Chung and Seinfeld, 2002; Liao et al., 2007),

$$VOC_i + OX_1 \rightarrow \alpha_{i,1,1}SOG_{i,1,1} + \alpha_{i,1,2}SOG_{i,1,2} \longleftrightarrow SOAs \quad (3)$$

$$VOC_i + OX_2 \rightarrow \alpha_{i,2,3}SOG_{i,2,3} \longleftrightarrow SOAs \quad (4)$$

ACPD
10, 19811–19844, 2010

where $\alpha_{i,j,k}$ (i=1–6; j=1–2; k=1–3) are the mass-based Stoichiometric yield. $\alpha_{i,j,k}$ value along with equilibrium partition coefficient $K_{i,j,k}$ at reference temperature (T_{ref}) for each $\text{SOG}_{i,j,k}$ can be found in Griffin et al. (1999) and Kroll et al. (2006).

The fractions of total secondary organic products (SOG+SOA) in gaseous and particulate phase depend on the products' effective saturation concentrations C^* (in $\mu\text{g}\,\text{m}^{-3}$) which is the inverse of $K_{i,j,k}$ (Donahue et al., 2006). The temperature dependence of C^* can be determined by the Clausius-Clapeyron equation:

$$C_T^* = C_{T_{\text{ref}}}^* \frac{T_{\text{ref}}}{T} \exp\left[\frac{\Delta H}{R}\left(\frac{1}{T_{\text{ref}}} - \frac{1}{T}\right)\right] \quad (5)$$

where ΔH is the enthalpy of vaporization and R is the gas constant. In this study, ΔH (in $\text{kJ}\,\text{mole}^{-1}$) for different SOGs are calculated according to the parameterization given in Donahue et al. (2006).

As can be expected, C^* have a strong temperature dependence and have a large range of variations for different SOGs. Table 1 gives $\alpha_{i,j,k}$ value for each $\text{SOG}_{i,j,k}$ and their C^* values at T=290 K. C^* as a function of T is shown in Fig. 1. According to their C^*, we group SOGs into two classes: semi-volatile SOG (SV-SOG) and medium-volatile SOG (MV-SOG). SV-SOG includes the first oxidation product of VOC_i by O_3+OH, while MV-SOG includes the second oxidation product of VOC_i by O_3+OH and the oxidation product of VOC_i by NO_3.

As discussed in the Introduction, it is important to extend the above described 2-product SOA formation model so that it can take into account the SOG aging process which has been observed in more recent atmospheric and the laboratory measurements (e.g., Donahue et al., 2006; Jimenez et al., 2009). Additionally, the vapor pressures of SV-SOG and MV-SOG are too high to directly condense on freshly nucleated sulfate particles and it becomes necessary to predict the concentration of condensable SOGs so that the kinetic condensation process can be considered.

Figure 2 is a schematic illustration of particle formation and growth process as well as the oxidation aging process. H_2SO_4 gas is well recognized to be involved in nucleation and also contributes to particle growth through condensation. NH_3 and HNO_3

ACPD
10, 19811–19844, 2010

can be uptaken by sulfate particles through thermodynamic equilibrium and contribute to aerosol growth and mass. Particles of various sizes are generally in equilibrium with H_2O vapor and the hygroscopic growth factor depends on particle compositions. We extend the 2-product model by adding a third component representing low-volatile secondary organic gases (LV-SOG) resulting from oxidation aging. The vapor pressure of this LV-SOG is in the range of ~0.01–1 ppt and thus is low enough to condense on pre-existing particles. LV-SOG is important for particle growth because it not only directly contributes to the condensation growth but also acts as absorbing mass and enables the particles to uptake SV-SOG and MV-SOG via absorptive partition. The vapor pressures of SV-SOG and MV-SOG are typically in the range of 1 ppt–1 ppb and 0.1 ppb–100 ppb, respectively. HV-SOG with C^* in the range of ~10 ppb–10 ppm, generally considered to be unimportant for SOA formation because of their high vapor pressure, could provide additional sources for MV-SOG as a result of aging and thus contribute to SOA formation. HV-SOG is not included in the present model because of the lack of yield and C^* information but can be readily incorporated into our scheme when relevant data becomes available.

The vapor pressure of sulfuric acid gas over the flat surface of a H_2SO_4-H_2O binary solution at T=290 K and RH=50% is ~0.001 ppt. It is clear that $C^*_{H_2SO_4} < C^*_{LV\text{-}SOG} < C^*_{SV\text{-}SOG} < C^*_{MV\text{-}SOG} < C^*_{HV-SOG}$. H_2SO_4 vapor pressure is low enough to enable it to be involved in the nucleation process. LV-SOG generally has a substantial contribution to the growth of nucleated particles larger than ~3 nm, but their contribution to the growth of sub-3 nm particles is likely limited as a result of the Kelvin effect (Yu and Turco, 2008; Wang et al., 2010). LV-SOA on secondary particles resulting from the condensation of LV-SOG serves as the absorbing mass (M_{absorb}) and allow SV-SOGs and MV-SOGs to be uptaken through partitioning which further grow the secondary particles.

The equations governing the changes of LV-, SV-, and MV-SOG concentrations ($C_{LV\text{-}SOG}$, $C_{SV\text{-}SOG}$, $C_{MV\text{-}SOG}$) at a given grid box associated with chemical and microphysical processes are,

$$dC_{MV\text{-}SOG}/dt = P_{VOC} - K_{ag}[OH]\xi_{MV->SV}C_{MV\text{-}SOG} - L_{par} \quad (6)$$

ACPD
10, 19811–19844, 2010

$$dC_{SV\text{-}SOG}/dt = P_{VOC} + K_{ag}[OH]\xi_{MV->SV}C_{MV\text{-}SOG} - K_{ag}[OH]\xi_{SV->LV}C_{SV\text{-}SOG} - L_{par} \quad (7)$$

$$dC_{LV\text{-}SOG}/dt = K_{ag}[OH]\xi_{SV->LV}C_{SV\text{-}SOG} - L_{cond} \quad (8)$$

where P_{VOC} is the VOC oxidation production term (Eqs. 3 and 4), L_{par} is the loss to aerosol via partitioning, and L_{cond} is the loss to particle via condensation. K_{ag} is the oxidation aging rate (Jimenez et al., 2009). In the present SOA formation model, there are 6 SV-SOGs and 10 MV-SOGs considered (see Table 1). The transfer of mass from MV-SOG to SV-SOG is based on the category of the parent VOC_i (i.e, from MV-$SOG_{i,1,2}$ and MV-$SOG_{i,2,3}$ to SV-$SOG_{i,1,1}$, i=1–6). All the oxidation products of SV-SOGs are lumped into one LV-SOG. Following Jimenez et al. (2009), we use a K_{ag} value of 3×10^{-11} cm^3 s^{-1} in this study. $\xi_{MV->SV}$ is the fraction of each MV-SOG that can be oxidized to become the corresponding SV-SOG, and $\xi_{SV->LV}$ is the fraction of each SV-SOG that can be oxidized to become LV-SOG. It should be noted that transport and deposition of LV-, SV-, and MV- SOGs, which are not included in Eqs. (6)–(8), are considered in the GEOS-Chem model.

The values of $\xi_{MV->SV}$ (or $\xi_{SV->LV}$) depend on the decrease of SOG vapor pressure due to oxidation and the ratios of C^*_{MV} to C^*_{SV} (or C^*_{SV} to C^*_{LV}) which differ for different SOGs and vary with temperature. To determine $\xi_{MV->SV}$ and $\xi_{SV->LV}$ is a challenging task. Each SOG group may contain hundreds of different organic species with vapor pressures distributed around the mean value. To account for the spreading of vapor pressures around the averaged values, we represent each SV-SOG or MV-SOG group with a normalized distribution.

$$f_{SOG}(C^*) = \frac{dF_{SOG}(C^*)}{d\log C^*} = \frac{1}{\sqrt{2\pi}\ln\sigma_g} e^{\left[\frac{\left(\ln C^* - \ln \overline{C}^*_{SOG}\right)^2}{2\ln^2\sigma_g}\right]} \quad (9)$$

where $dF_{SOG}(C^*)=f_{SOG}(C^*)\times d\log C^*$ is the fraction of SOG within $d\log C^*$. σ_g is the geometric standard geometric deviation and $\overline{C}^*_{SOGi}$ is the median C^*.

ACPD
10, 19811–19844, 2010

Figure 3 show the normalized distributions ($f_{SOG}(C^*)$) of various SOGs at T=295 K. The vapor pressure ranges of LV-, SV-, and MV-SOGs are also indicated in the figure. One benefit of normalized distribution is that it allows the integrated fraction of SOG below certain vapor pressure values to change smoothly with temperature, which should be the case in the real atmosphere. It is clear from Fig. 3 that C^*_{MV}/C^*_{SV} and C^*_{SV}/C^*_{LV} vary substantially for different SOGs. To account for the effect of such variations on oxidation aging rates, we parameterize $\xi_{MV->SV}$ and $\xi_{SV->LV}$ values as,

$$\xi_{SV->LV} = \int_0^{\varphi\overline{C^{upp}_{LV}}} f_{SV\text{-}SOG} \mathrm{dlog}C \quad (10)$$

$$\xi_{MV->SV} = \int_0^{\varphi\overline{C^{*}_{SV}}} f_{MV\text{-}SOG} \mathrm{dlog}C \quad (11)$$

where f_{SOG} is the normalized distribution of each SOG group (Eq. 9, also see Fig. 3). $\overline{C^{upp}_{LV}}$ is the upper limit of LV-SOG vapor pressure (fixed to be 0.01 μg m^{-3} in this study). $\overline{C^*_{SV}}$ is the geometric mean vapor pressure of SV-SOG under a given temperature. φ is the ratio of the vapor pressure of SOG to that of its one generation oxidation product. $\varphi\overline{C^{upp}_{LV}}$ and $\varphi\overline{C^*_{SV}}$ are the cut-off vapor pressures below which the SV-SOG and MV-SOG can be oxidized (in one generation) to become LV-SOG and SV-SOG, respectively. According to the structure activity relationships described by Pankow and Asher (2008), added –OH functionality decreases the C^* of an organic backbone by a factor of ~10^2, while added =O functionality decreases C^* by a factor of 10. Following the value suggested in Jimenez et al. (2009), we assume that each generation of oxidation by OH adds one oxygen atom and reduces C^* by 1.5 decades (i.e, φ=$10^{1.5}$).

ACPD
10, 19811–19844, 2010

3 Global SOA formation and particle growth modeling with GEOS-Chem+APM

The model employed in this study is the GEOS-Chem model with an advanced particle microphysics (APM) model incorporated (Yu and Luo, 2009). The GEOS-Chem model is a global 3-D model of atmospheric composition driven by assimilated meteorological data from the NASA Goddard Earth Observing System 5 (GEOS-5), has been developed and used by many research groups, and contains a number of state-of-the-art modules treating various chemical and aerosol processes (e.g., Bey et al., 2001; Martin et al., 2003; Park et al., 2004; Evans and Jacob, 2005; Liao et al., 2007) with up-to-date key emission inventories (e.g., Guenther et al., 2006; Bond et al., 2007; Zhang et al., 2009). A detailed description of the GEOS-Chem (including various emission sources, chemistry and aerosol schemes) can be found in the model webpage (http://acmg.seas.harvard.edu/geos). The APM model will be incorporated into the standard version of GEOS-Chem in the near future. The details of aerosol representation and processes in GEOS-Chem+APM can be found in Yu and Luo (2009).

In this work, we implement the new SOA formation scheme described in Sect. 2 in GEOS-Chem+APM and use the updated model to study the effect of oxidation aging and SOA explicit condensation on simulated particle properties in the global scale. The co-condensation of H_2SO_4 and LV-SOG on size-resolved secondary particles is explicitly simulated (Yu and Turco, 2008) and the scavenging of these precursors by primary particles is also considered. To reduce the number of tracers in the model, we lump all LV-SOA on secondary particle (SP) of different sizes into one tracer (SP_LV) and redistribute SP_LV into different sizes according to SP surface area when needed. Similar to the amount of sulfate coated on various primary particles (Yu and Luo, 2009), we use four additional tracers (dust_LV, BC_LV, POC_LV, and salt_LV) to track the amount of LV-SOA coated on various primary particles (i.e., dust, black carbon, primary organic carbon, and sea salt) as a result of condensation and coagulation. The implementation of a new SOA formation scheme adds 6 additional tracers (5 for LV-SOA on different types of particles and 1 for LV-SOG), with a small increase in the computing cost (<5%). The schemes within APM are designed with special emphasis on capturing the

ACPD
10, 19811–19844, 2010

main properties of atmospheric particles important for their direct and indirect radiative forcing while keeping computational costs low.

The GEOS-Chem v8-01-03 used in Yu and Luo (2009) has been updated to v8-02-03 for the present simulation. All the annual mean results given below are based on simulations for year 2005 (2-month spin up time) with a horizontal resolution of $4^\circ \times 5^\circ$ and 47 vertical layers up to 0.01 hpa (GEOS-5 meteorological fields). We also run the model at a horizontal resolution of $2^\circ \times 2.5^\circ$ from 1 March 2005–31 May 2005 while the output for May 2005 was saved every 30 min for comparisons with size distribution measurements at Hyytiälä, Findland. The oceanic α-pinene emission indicated by ship measurements is not considered in the present study due to the large unresolved difference between the total fluxes derived from "top-down" and "bottom-up" approaches (Luo and Yu, 2010). New particle formation is calculated based on an ion-mediated nucleation mechanism (Yu, 2010) which is based on state-of-the-art thermodynamic and laboratory data (Yu, 2010) and has been validated against well constrained case studies of nucleation events observed in boreal forests (Yu and Turco, 2008). Previous global modeling studies indicate that the IMN mechanism appears to reasonably account for total number concentrations of particles larger than ~4 nm and ~10 nm observed in different parts of the troposphere (Yu and Luo, 2009; Yu et al., 2010).

Figure 4 shows the horizontal distributions of annual mean values of H_2SO_4 gas concentration ($[H_2SO_4]$), LV-SOG concentration ([LV-SOG]), and the ratio of [LV-SOG] to $[H_2SO_4]$ in the boundary layer (averaged within first seven model layers above Earth's surface: 0–1 km). [LV-SOG] is a factor of ~2–20 higher than $[H_2SO_4]$ over many parts of the continents but is lower or close to $[H_2SO_4]$ in East Asia, Middle and Southern Europe, and the Eastern US where anthropogenic SO_2 sources are strong. It should be noted that the aging of anthropogenic VOCs is not included in the present SOA formation model described in Sect. 2. There exists evidence that anthropogenic VOCs can age and contribute to SOA formation in source regions (Volkamer et al., 2006; Robinson et al., 2007). Thus, [LV-SOG] in East Asia, Middle and Southern Europe, and the Eastern United States might be substantially higher than the values given in Fig. 4b

ACPD
10, 19811–19844, 2010

when the oxidation aging of anthropogenic VOCs is included. It is clear from Fig. 4 that the high [LV-SOG] is limited to continents and [LV-SOG] over oceans is generally much lower than [H_2SO_4]. This is a result of the short life of biogenic VOCs and lack of LV-SOG production over oceans. It is noteworthy that a number of recent studies indicate the oceanic sources of isoprene and α-pinene (Meskhidze and Nenes, 2006; Roelofs, 2008; Yassaa et al., 2008; Luo and Yu, 2009), which are not included in this study because of the large difference in the source strength estimated from "bottom-up" and "top-down" methods (Arnold et al., 2009; Gantt et al., 2009; Luo and Yu, 2009). Depending on the source strength of oceanic VOC emission, [LV-SOG] over oceans could increase substantially. Further research is needed to characterize the contributions of the aging of anthropogenic VOCs and oceanic VOC emissions to the LV-SOG concentration and the associated impact on particle properties.

As pointed out in Sect. 2, the vapor pressure of LV-SOG (~0.01–1 ppt) is low enough for explicit condensation. In this study, we assume that LV-SOG has an average vapor pressure of 0.1 ppt (equivalent to $\sim 3.6\times10^6\,cm^{-3}$) and the co-condensing of H_2SO_4 and LV-SOG is explicitly resolved in the model. Figure 5 shows the simulated particle size distribution evolution based on previous 2-product SOA formation model (i.e., no oxidation aging and explicit condensation of LV-SOG) and extended SOA formation model described in Sect. 2 in a boreal forest site (Hyytiälä, Finland) during May 2005. For comparison, the observed size distribution evolution for the same location during the same period is also given (data from the CREATE Aerosol Database). The long-term continuous particle size distribution measurements in Hyytiälä by Kulmala and colleagues provide excellent data illustrating the formation and growth of atmospheric particles and have been analyzed in a number of previous publications (Laakso et al., 2004; Kulmala et al., 2004; Ehn et al., 2007; Laaksonen et al., 2008). It can be clearly seen from Fig. 5 that the condensation of LV-SOG is important to bring the simulations closer to observations. Without LV-SOG, H_2SO_4 can only grow nucleated particles to around ~10–30 nm within a day. In contrast, the participation of LV-SOG (plus the absorbing of SV-SOG and MV-SOG) drives the particles to ~40–

ACPD
10, 19811–19844, 2010

100 nm within the day. Our simulations indicate that H_2SO_4 account for <~20% of the growth rate of nucleated particles in the boreal forest, which is consistent with the observations (Kulmala et al., 2004). It is interesting to note that, when LV-SOG condensation is considered, nucleation events are shorter and generate fewer new particles. This is a result of increased particle surface area and reduced [H_2SO_4] associated with enhanced growth rates. A comparison of Fig. 5b with Fig. 5c shows that the overall agreement between simulated (with LV-SOG condensation) and observed size distributions is reasonable, indicating that the new extended SOA formation model may be able to capture some major processes of SOG oxidation aging and particle growth. The model reproduces a large fraction of strong nucleation events (days 122–123, 131–134, 140, 148) and weak or non-nucleation periods (days 124–130, 142–147, 150–152). The weak or non-nucleation periods appear to follow previous strong nucleation and growth events, suggesting some kind of particle number self-limiting process in the atmosphere. There exist some differences in the simulated and observed nucleation and growth rates on some days, which may be associated with the coarse model horizontal resolution ($2^\circ \times 2.5^\circ$ grid box versus a fixed site) and uncertainties in various processes (emissions, meteorology, chemistry, microphysics, etc.). Overall, the results are quite encouraging. It is clear from Fig. 5 that, consistent with various observations (Kulmala et al., 2004; Kuang et al., 2010), the consideration of LV-SOG condensation is critical and the extended SOA formation model may significantly advance the model's ability to simulate particle formation and growth in the troposphere.

The effect of the new SOA formation scheme on simulated total SOA mass in the boundary layer is given in Fig. 6. Without LV-SOG condensation (Fig. 6a), SOA can only form via absorptive partitioning with primary organic carbon (POC) and the annual mean SOA mass is generally <0.3μg m^{-3} in most parts of the boundary layer except in the Eastern United States (0.3–0.7 μg m^{-3}), Eastern Asia (0.3–2 μg m^{-3}), Australia (0.3–0.5), Sothern Africa and Southern America (up to 5 μg m^{-3}). With the new SOA formation scheme that takes into account SOG oxidation aging and LV-SOG condensation, annual mean SOA mass in the boundary layer over the whole globe in-

ACPD
10, 19811–19844, 2010

creases significantly, by a factor of 2–10 in many parts of the boundary layer (Fig. 6c). Annual mean SOA mass reaches above 1 $\mu g\,m^{-3}$ in most parts of main continents, except in the high latitude Arctic and Antarctic regions (<0.3 $\mu g\,m^{-3}$). The enhancement over the oceans is also significant although the absolute SOA mass is still quite low (<~0.1 $\mu g\,m^{-3}$). Total SOA mass obtained at multiple surface locations in the Northern Hemisphere based on factor analysis of AMS data (FA-AMS), as presented in Jimenez et al. (2009), is largely in the range of 1–8 $\mu g\,m^{-3}$. The annual mean SOA mass presented in Fig.6 cannot be directly compared to the AMS data summarized in Jimenez et al. (2009), because most AMS measurements lasted for a few weeks and many measurements were in the urban areas. Detailed comparisons of simulated SOA mass (at higher horizontal model resolution and during the specific periods of various observations) with AMS observations will be carried out and reported in future publications.

Figure 7a shows the horizontal distributions of annual mean number concentrations of condensation nuclei larger than 10 nm (CN10) in the lower boundary layer (0–0.4 km) simulated with the new SOA formation model described in this paper. Overlaid on Fig. 7a for comparison (symbols) are the annual or multiple-year averaged CN10 values observed at 21 surface sites around the globe, with a more specific comparison of simulated CN10 with observed values given in Fig. 8. The sources of CN10 data include CREATE Aerosol Database at NILU (tarantula.nilu.no/projects/ccc/create/index.htm), World Data Centre for Aerosols (wdca.jrc.ec.europa.eu), NOAA ESRL/GMD Aerosol Database (www.cmdl.noaa.gov/aero), Dal Maso et al. (2008), Ziemba et al. (2006), Laakso et al. (2008), Suni et al. (2008), Venzac et al. (2008), Komppula et al. (2009), and Kivekäs et al. (2009). More details of these data can be found in Yu and Luo (2009). The impact of including LV-SOG condensation on the annual mean CN10 in the lower boundary layer (0–0.4 km) is presented in Fig. 7b. Enhanced growth rate associated with LV-SOG condensation has two effects on CN10: 1) it increases the fractions of nucleated particles growing beyond 10 nm; 2) it increases the surface area of particles (or condensation sink) which leads to a reduction in $[H_2SO_4]$ and nucleation rates. Our

ACPD
10, 19811–19844, 2010

simulations indicate that, in most parts of the lower boundary layer, the second effect exceeds the first effect and the inclusion of LV-SOG condensation decreases CN10 by 3–30% (Fig. 7b). In terms of comparison with observed CN10 values, the inclusion of LV-SOG condensation slightly enhances the agreement (Fig. 8). Both cases (with and without LV-SOG condensation) appear to capture the annual mean CN10 values within a factor of ~2. The results presented in Figs. 5 and 7 highlight the necessity to use aerosol measurements in addition to CN10 data (such as size distributions, etc.) to validate global aerosol models.

Figure 9 gives total CCN concentration at a water supersaturation ratio of 0.2% (CCN0.2) in the lower troposphere (lowest 2 km, averaged within the lowest 14 model layers) for the case with LV-SOG condensation, and percentage changes in CCN0.2 when compared to the case without SOG oxidation aging and LV-SOG condensation. As can be seen from Fig. 9a, annual mean CCN0.2 values in the lower troposphere over major continents generally exceed ~200 cm^{-3} with the highest values reaching above 1000 cm^{-3}, while those over oceans are generally below 100 cm^{-3} with the lowest values dipping under 40 cm^{-3}. It is clear from Fig. 9b that SOG oxidation aging and LV-SOG condensation substantially increases CCN0.2 values in most parts of the lower troposphere, ranging from 3–10% over a large fraction of oceans to more than 100% over some parts of South America. The enhancement is relatively lower over oceans because of the short lifetime of biogenic VOCs and lower LV-SOG concentrations over oceans (Fig. 4). Over the major continents, the enhancement is relatively low (<~20%) in the regions of high CCN0.2 values (>~450 cm^{-3}) such as the Eastern United States, Eastern Asian, and Europe. The regions of the highest CCN0.2 enhancement (>50%) include Northwest America, Indonesia, Australia, Southern Africa and America and their associated outflows, where the CCN0.2 values are in the range of several tens to several hundreds per cm^3. We also see a slight decrease (<~10%) of CCN0.2 in the Middle East and Northern Africa, most likely a result of the reduction of secondary particles transported to these regions (Fig. 7) and the absence of LV-SOG in the area (Fig. 4).

ACPD
10, 19811–19844, 2010

CCN concentrations are well known to be important for aerosol indirect radiative forcing. Based on the relationship between cloud albedo (A) and CCN concentration (N) given in Platnick and Twomey (1994) ($\Delta A/A=(1-A)/3\times\Delta N/N$), a 10% increase in CCN concentrations can lead to ~2% increase in average cloud albedo (assuming global average A of 0.42, Han et al. (2001). Since clouds on average reflect about 50 $W\,m^{-2}$ of incoming solar radiation back to space (Hartmann, 1993), a 2% increase in the average cloud albedo could lead to a radiative cooling of ~1 $W\,m^{-2}$. Thus, the first indirect radiative forcing associated with SOA formation could be well above 1 $W\,m^{-2}$ over major continents. While these estimations are crude, they do indicate the importance of properly representing the SOA formation and its contribution to particle growth and CCN abundance within global aerosol models.

4 Summary and discussion

The contribution of secondary organic aerosol (SOA) to particle growth, size, and mass is one of major uncertainties in current regional and global aerosol simulations. The volatility changes of secondary organic gases (SOGs) arising from the aging process as well as the contribution of low volatile SOGs to the condensational growth of secondary particles have been found to be important in recent laboratory and field measurements but are poorly represented in global aerosol models. In this study, we extend the widely used 2-product SOA formation model so that it can consider the aging process as well as the kinetic condensation of low-volatile SOGs. According to their effective vapor pressure, we group SOGs from biogenic VOC oxidation into two classes: semi-volatile SOG (SV-SOG) and medium-volatile SOG (MV-SOG). Thereafter, we extend the 2-product model by adding a third component representing low-volatile SOG (LV-SOG) and design a scheme to transfer MV-SOG to SV-SOG and SV-SOG to LV-SOG as a result of oxidation aging. The vapor pressure of this LV-SOG is in the range of ~0.01–1 ppt and is low enough to enable it to directly condense on pre-existing particles. The extended SOA formation model has been implemented in a recently

ACPD
10, 19811–19844, 2010

developed size-resolved (sectional) global aerosol model GEOS-Chem+APM. The concentration of LV-SOG ([LV-SOG]) is predicted and the co-condensation of H_2SO_4 and LV-SOG on size-resolved secondary particles is explicitly simulated, along with the scavenging of these precursors by primary particles.

Our simulations indicate that [LV-SOG] is generally a factor of ~2–20 higher than [H_2SO_4] over many parts of the continents and significantly enhance the growth rates of nucleated particles. A comparison of the simulated and observed evolution of particle size distributions in a boreal forest site (Hyytiälä, Finland) clearly shows that the condensation of oxidation aging and LV-SOG is important to bring the simulations close to the observations. With the new SOA formation scheme, annual mean SOA mass in the boundary layer over the whole globe increases significantly (by a fact of 2–10 in many parts of the boundary layer) and reaches above 1 μg m^{-3} in most part of main continents. We also find that LV-SOG condensation increases particle surface area, reduces [H_2SO_4], and thus decreases the formation rates of new particles. As a result, the concentration of condensation nuclei larger than 10 nm (CN10) decreases by 3–30% in most parts of the lower boundary layer when LV-SOG condensation is included. A comparison of simulated annual mean CN10 values with the annual or multiple-year averaged CN10 values observed in 21 surface sites around the globe indicates that the inclusion of LV-SOG condensation slightly enhances the agreement but both cases (with and without LV-SOG condensation) appear to be able to capture the observed annual mean CN10 values within a factor of ~2. SOG oxidation aging and LV-SOG condensation substantially increase CCN0.2 values in most parts of the lower troposphere, ranging from 3–10% over a large fraction of oceans to more than 100% over some parts of South America. Over the major continents, the enhancement is relatively weak (<~20%) in the regions of high CCN0.2 values (>~450 cm^{-3}) and relatively strong (>50%) in the region low CCN0.2 (several tens to several hundreds per cm^3).

Our study suggests that the aging of VOC oxidation products and their contribution of particle growth could substantially increase CCN concentrations in the lower tropo-

ACPD
10, 19811–19844, 2010

sphere and enhance aerosol indirect radiative forcing. In view of the strong dependence of aerosol indirect radiative forcing on CCN concentrations, our study highlights the importance for global aerosol models to explicitly take into account and reduce uncertainty associated with the oxidation aging of SOGs and their contribution of particle growth. Further research is needed to reduce the uncertainty in SOG oxidation aging rates, characterize the contributions of the aging of anthropogenic VOCs and oceanic VOC emissions to the LV-SOG concentration, improve the representation of SOGs and size-resolved SOA, as well as validate the model predictions with more detailed measurements.

Acknowledgements. The author thanks Dr Gan Luo (University at Albany) for assistance in running the GEOS-Chem model. The GEOS-Chem model is managed by the Atmospheric Chemistry Modeling Group at Harvard University with support from the NASA Atmospheric Chemistry Modeling and Analysis Program. The author thanks Professor Markku Kulmala (University of Helsinki) for making their particle size distribution data available via CREATE Aerosol Database at NILU. This study is supported by NASA under grant NNX08AK48G and NSF under grant 0942106.

References

Bey, I., Jacob, D. J., Yantosca, R. M., et al.: Global modeling of tropospheric chemistry with assimilated meteorology: model description and evaluation, J. Geophys. Res., 106, 23073–23096, 2001.

Bond, T. C., Bhardwaj, E., Dong, R., Jogani, R., Jung, S., Roden, C., Streets, D. G., and Trautmann, N. M.: Historical emissions of black and organic carbon aerosol from energy-related combustion, 1850–2000, Global Biogeochem. Cycles, 21, GB2018, doi:10.1029/2006GB002840, 2007.

Chung, S. H. and Seinfeld, J. H.: Global distribution and climate forcing of carbonaceous aerosols, J. Geophys. Res., 107, 4407, doi:10.1029/2001JD001397, 2002.

Dal Maso, M., Hyvarinen, A., Komppula, M., et al.: Annual and interannual variation in boreal forest aerosol particle number and volume concentration and their connection to particle formation, Tellus, 60B, 495–508, 2008.

ACPD

10, 19811–19844, 2010

Donahue, N. M., Robinson, A. L., Stanier, C. O., and Pandis, S. N.: Coupled partitioning, dilution, and chemical aging of semivolatile organics, Environ. Sci. Technol., 40, 2635–2643, 2006.

Ehn, M., Petäjä, T., Aufmhoff, H., Aalto, P., Hämeri, K., Arnold, F., Laaksonen, A., and Kulmala, M.: Hygroscopic properties of ultrafine aerosol particles in the boreal forest: diurnal variation, solubility and the influence of sulfuric acid, Atmos. Chem. Phys., 7, 211–222, doi:10.5194/acp-7-211-2007, 2007.

Evans, M. J. and Jacob, D. J.: Impact of new laboratory studies of N_2O_5 hydrolysis on global model budgets of tropospheric nitrogen oxides, ozone, and OH, Geophys. Res. Lett., 32, L09813, doi:10.1029/2005GL022469, 2005.

Griffin, R. J., Cocker III, D. R., Flagan, R. C., and Seinfeld, J. H.: Organic aerosol formation from the oxidation of biogenic hydrocarbons, J. Geophys. Res., 104, 3555–3567, 1999.

Guenther, A., Karl, T., Harley, P., Wiedinmyer, C., Palmer, P. I., and Geron, C.: Estimates of global terrestrial isoprene emissions using MEGAN (Model of Emissions of Gases and Aerosols from Nature), Atmos. Chem. Phys., 6, 3181–3210, doi:10.5194/acp-6-3181-2006, 2006.

Hallquist, M., Wenger, J. C., Baltensperger, U., Rudich, Y., Simpson, D., Claeys, M., Dommen, J., Donahue, N. M., George, C., Goldstein, A. H., Hamilton, J. F., Herrmann, H., Hoffmann, T., Iinuma, Y., Jang, M., Jenkin, M. E., Jimenez, J. L., Kiendler-Scharr, A., Maenhaut, W., McFiggans, G., Mentel, Th. F., Monod, A., Prévôt, A. S. H., Seinfeld, J. H., Surratt, J. D., Szmigielski, R., and Wildt, J.: The formation, properties and impact of secondary organic aerosol: current and emerging issues, Atmos. Chem. Phys., 9, 5155–5236, doi:10.5194/acp-9-5155-2009, 2009.

Han, Q., Rossow, W. B., Chou, J., and Welch, R. M.: Global survey of the relationships of cloud albedo and liquid water path with droplet size using ISCCP, J. Climate, 11, 1516–1528, 1998.

Hartmann, D. L.: Radiative effects of clouds on Earth's climate, in: Aerosol-Cloud-Climate Interactions, edited by: Bobbs, P. V., Academic Press, Harcourt Brace & Company, New York, 1993.

Heald, C. L., Jacob, D. J., Park, R. J., et al.: A large organic aerosol source in the free troposphere missing from current models, Geophys. Res. Lett., 32, L18809, doi:10.1029/2005GL023831, 2005.

Henze, D. K. and Seinfeld, J. H.: Global secondary organic aerosol from isoprene oxidation,

ACPD

10, 19811–19844, 2010

Geophys. Res. Lett., 33, L09812, doi:10.1029/2006GL025976, 2006.
Jimenez, J. L., Canagaratna, M. R., Donahue, N. M., Prévôt, A. S. H., Zhang, Q., et al.: Evolution of organic aerosols in the atmosphere, Science, 326, 1525, doi:10.1126/science.1180353, 2009.
Kivekäs, N., Sun, J., Zhan, M., Kerminen, V.-M., Hyvärinen, A., Komppula, M., Viisanen, Y., Hong, N., Zhang, Y., Kulmala, M., Zhang, X.-C., Deli-Geer, and Lihavainen, H.: Long term particle size distribution measurements at Mount Waliguan, a high-altitude site in inland China, Atmos. Chem. Phys., 9, 5461–5474, doi:10.5194/acp-9-5461-2009, 2009.
Komppula, M., Lihavainen, H., Hyvärinen, A.-P., et al.: Physical properties of aerosol particles at a Himalayan background site in India, J. Geophys. Res., 114, D12202, doi:10.1029/2008JD011007, 2009.
Kroll, J. H. and Seinfeld, J. H.: Chemistry of secondary organic aerosol: formation and evolution of low-volatility organics in the atmosphere, Atmos. Environ., 42, 3593–3624, 2008.
Kuang, C., Riipinen, I., Sihto, S.-L., Kulmala, M., McCormick, A. V., and McMurry, P. H.: An improved criterion for new particle formation in diverse atmospheric environments, Atmos. Chem. Phys. Discuss., 10, 491–521, doi:10.5194/acpd-10-491-2010, 2010.
Kulmala, M., Vehkamäki, H., Petäjä, T., Dal Maso, M., Lauri, A., Kerminen, V.-M., Birmili, W., and McMurry, P.: Formation and growth rates of ultrafine atmospheric particles: a review of observations, J. Aerosol Sci., 35, 143–176, 2004.
Laakso, L., Anttila, T., Lehtinen, K. E. J., Aalto, P. P., Kulmala, M., Hõrrak, U., Paatero, J., Hanke, M., and Arnold, F.: Kinetic nucleation and ions in boreal forest particle formation events, Atmos. Chem. Phys., 4, 2353–2366, doi:10.5194/acp-4-2353-2004, 2004.
Laakso, L., Laakso, H., Aalto, P. P., Keronen, P., Petäjä, T., Nieminen, T., Pohja, T., Siivola, E., Kulmala, M., Kgabi, N., Molefe, M., Mabaso, D., Phalatse, D., Pienaar, K., and Kerminen, V.-M.: Basic characteristics of atmospheric particles, trace gases and meteorology in a relatively clean Southern African Savannah environment, Atmos. Chem. Phys., 8, 4823–4839, doi:10.5194/acp-8-4823-2008, 2008.
Laaksonen, A., Kulmala, M., O'Dowd, C. D., Joutsensaari, J., Vaattovaara, P., Mikkonen, S., Lehtinen, K. E. J., Sogacheva, L., Dal Maso, M., Aalto, P., Petäjä, T., Sogachev, A., Yoon, Y. J., Lihavainen, H., Nilsson, D., Facchini, M. C., Cavalli, F., Fuzzi, S., Hoffmann, T., Arnold, F., Hanke, M., Sellegri, K., Umann, B., Junkermann, W., Coe, H., Allan, J. D., Alfarra, M. R., Worsnop, D. R., Riekkola, M. -L., Hyötyläinen, T., and Viisanen, Y.: The role of VOC oxidation products in continental new particle formation, Atmos. Chem. Phys., 8, 2657–2665,

ACPD
10, 19811–19844, 2010

doi:10.5194/acp-8-2657-2008, 2008.
Liao, H., Henze, D. K., Seinfeld, J. H., Wu, S., and Mickley, L. J.: Biogenic secondary organic aerosol over the United States: comparison of climatological simulations with observations, J. Geophys. Res., 112, D06201, doi:10.1029/2006JD007813, 2007.
Luo, G. and Yu, F.: A numerical evaluation of global oceanic emissions of α-pinene and isoprene, Atmos. Chem. Phys., 10, 2007–2015, doi:10.5194/acp-10-2007-2010, 2010.
Martin, R. V., Jacob, D. J., Yantosca, R. M., Chin, M., and Ginoux, P.: Global and regional decreases in tropospheric oxidants from photochemical effects of aerosols, J. Geophys. Res., 108, 4097, doi:10.1029/2002JD002622, 2003.
Odum, J. R., Hoffmann, T., Bowman, F., Collins, D., Flagan, R. C., and Seinfeld, J. H.: Gas/particle partitioning and secondary organic aerosol yields, Environ. Sci. Technol., 30, 2580–2585, 1996.
Pankow, J. F. and Asher, W. E.: SIMPOL.1: a simple group contribution method for predicting vapor pressures and enthalpies of vaporization of multifunctional organic compounds, Atmos. Chem. Phys., 8, 2773–2796, doi:10.5194/acp-8-2773-2008, 2008.
Pankow, J. F.: An absorption model of the gas/aerosol partitioning involved in the formation of secondary organic aerosol, Atmos. Environ., 28(6), 189–193, 1994.
Park, R. J., Jacob, D. J., Field, B. D., Yantosca, R. M., and Chin, M.: Natural and transboundary pollution influences on sulfate-nitrate-ammonium aerosols in the US: implications for policy, J. Geophys. Res., 109, D15204, doi:10.1029/2003JD004473, 2004.
Platnick, S. and Twomey, S.: Determining the susceptibility of cloud albedo to changes in droplet concentration with the advanced very high resolution radiometer, J. Appl. Meteorol., 33, 334–347, 1994.
Robinson, A. L., Donahue, N. M., Shrivastava, M. K., et al.: Rethinking organic aerosols: semivolatile emissions and photochemical aging, Science, 315, 1259–1262, 2007.
Rudich, Y., Donahue, N. M., and Mentel, T. F.: Aging of organic aerosol: bridging the gap between laboratory and field studies, Annu. Rev. Phys. Chem., 58, 321–352, 2007.
Schell, B., Ackermann, I. J., Hass, H., Binkowski, F. S., and Ebel, A.: Modeling the formation of secondary organic aerosol within a comprehensive air quality model system, J. Geophys. Res., 106, 28275–28293, 2001.
Seinfeld, J. H. and Pankow, J. F.: Organic atmospheric particulate material, Annu. Rev. Phys. Chem., 54, 121–140, 2003.
Suni, T., Kulmala, M., Hirsikko, A., Bergman, T., Laakso, L., Aalto, P. P., Leuning, R., Cleugh, H.,

ACPD
10, 19811–19844, 2010

Zegelin, S., Hughes, D., van Gorsel, E., Kitchen, M., Vana, M., Hõrrak, U., Mirme, S., Mirme, A., Sevanto, S., Twining, J., and Tadros, C.: Formation and characteristics of ions and charged aerosol particles in a native Australian Eucalypt forest, Atmos. Chem. Phys., 8, 129–139, doi:10.5194/acp-8-129-2008, 2008.

Tsigaridis, K. and Kanakidou, M.: Global modelling of secondary organic aerosol in the troposphere: a sensitivity analysis, Atmos. Chem. Phys., 3, 1849–1869, doi:10.5194/acp-3-1849-2003, 2003.

Venzac, H., Sellegri, K., Laj, P., et al.: High frequency new particle formation in the Himalayas, P. Natl. Acad. Sci. USA, 105, 15666–15671, 2008.

Volkamer, R., Jimenez, J. L., Martini, F. S., Dzepina, K., Zhang, Q., Salcedo, D., Molina, L. T., Worsnop, D. R., and Molina, M. J.: Secondary organic aerosol formation from anthropogenic air pollution: rapid and higher than expected, Geophys. Res. Lett., 33, L17811, doi:10.1029/2006GL026899, 2006.

Wang, L., Khalizov, A. F., Zheng, J., Xu, W., Lal, V., Ma, Y., and Zhang, R.: Atmospheric nanoparticles formed from heterogeneous reactions of organics, Nat. Geosci., 3, 238–242, doi:10.1038/ngeo778, 2010.

Yu, F. and Luo, G.: Simulation of particle size distribution with a global aerosol model: contribution of nucleation to aerosol and CCN number concentrations, Atmos. Chem. Phys., 9, 7691–7710, doi:10.5194/acp-9-7691-2009, 2009.

Yu, F. and Turco, R.: Case studies of particle formation events observed in boreal forests: implications for nucleation mechanisms, Atmos. Chem. Phys., 8, 6085–6102, doi:10.5194/acp-8-6085-2008, 2008.

Yu, F., Luo, G., Bates, T., Anderson, B., Clarke, A., Kapustin, V., Yantosca, R., Wang, Y., and Wu, S.: Spatial distributions of particle number concentrations in the global troposphere: simulations, observations, and implications for nucleation mechanisms, J. Geophys. Res., doi:10.1029/2009JD013473, in press, 2010.

Yu, F., Wang, Z., Luo, G., and Turco, R.: Ion-mediated nucleation as an important global source of tropospheric aerosols, Atmos. Chem. Phys., 8, 2537–2554, doi:10.5194/acp-8-2537-2008, 2008.

Yu, F.: Ion-mediated nucleation in the atmosphere: key controlling parameters, implications, and look-up table, J. Geophy. Res., 115, D03206, doi:10.1029/2009JD012630, 2010.

Zhang, Q., Jimenez, J. L., Canagaratna, M. R., Allan, J. D., Coe, H., et al.: Ubiquity and dom-

ACPD
10, 19811–19844, 2010

inance of oxygenated species in organic aerosols in anthropogenically-influenced Northern Hemisphere midlatitudes, Geophys. Res. Lett., 34, L13801, doi:10.1029/2007GL029979, 2007.

Zhang, Q., Streets, D. G., Carmichael, G. R., He, K. B., Huo, H., Kannari, A., Klimont, Z., Park, I. S., Reddy, S., Fu, J. S., Chen, D., Duan, L., Lei, Y., Wang, L. T., and Yao, Z. L.: Asian emissions in 2006 for the NASA INTEX-B mission, Atmos. Chem. Phys., 9, 5131–5153, doi:10.5194/acp-9-5131-2009, 2009.

Zhang, Y., Pun, B., Vijayaraghavan, K., Wu, S. Y., Seigneur, C., Pandis, S. N., Jacobson, M. Z., Nenes, A., and Seinfeld, J. H.: Development and application of the model of aerosol dynamics, reaction, ionization, and dissolution (MADRID), J. Geophys. Res., 109, D01202, doi:10.1029/2003JD003501, 2004.

Ziemba, L. D., Griffin, R. J., and Talbot, R. W.: Observations of elevated particle number concentration events at a rural site in New England, J. Geophys. Res., 111, D23S34, doi:10.1029/2006JD007607, 2006.

ACPD

10, 19811–19844, 2010

Table 1. Mass-based stoichiometric yield for semi-volatile products from the oxidation of major types of reactive biogenic volatile organic compounds (VOC_i, i=1–6) and the effective saturation concentrations (C^* in μg m^{-3}, inverse of equilibrium partition coefficient $K_{i,j,k}$) of these products at T=290 K. $\alpha_{i,j,k}$ value along with equilibrium partition coefficient $K_{i,j,k}$ at reference temperature (T_{ref}) for each $SOG_{i,j,k}$ can be found in Griffin et al. (1999a,b) and Kroll et al. (2006).

VOC_i	O_3+OH oxidation (OX_1)				NO_3 oxidation (OX_2)	
	Product type 1 (SV-SOG)		Product type 2 (MV-SOG)		Product type 3 (MV-SOG)	
	$\alpha_{i,1,1}$	$C^*_{i,1,1}$	$\alpha_{i,1,2}$	$C^*_{i,1,2}$	$\alpha_{i,2,3}$	$C^*_{i,2,3}$
i=1	0.067	0.45	0.354	25.05	1	6.00
i=2	0.239	1.64	0.363	19.92	1	6.00
i=3	0.069	0.64	0.201	31.02	1	6.00
i=4	0.067	0.37	0.135	12.50	1	6.00
i=5	1	1.99			1	6.00
i=6	0.029	0.31	0.232	63.68		

ACPD
10, 19811–19844, 2010

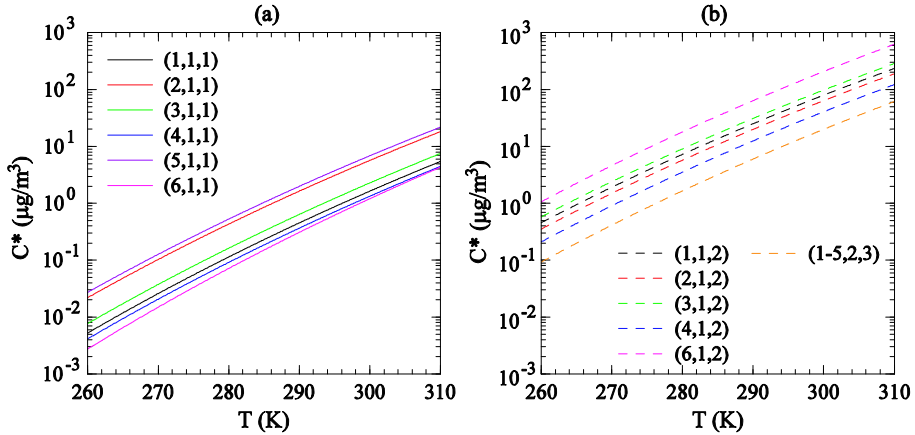

Fig. 1. The effect of temperature (T) on effective saturation concentrations (C^* in $\mu g\,m^{-3}$, inverse of equilibrium partition coefficient $K_{i,j,k}$) of 16 oxidation products from the oxidation of VOC_i (i=1–6) by OX_j (j=1–2). The numbers inside the parenthesis in the figure legend are (i,j,k) of each product. See text for more information.

ACPD
10, 19811–19844, 2010

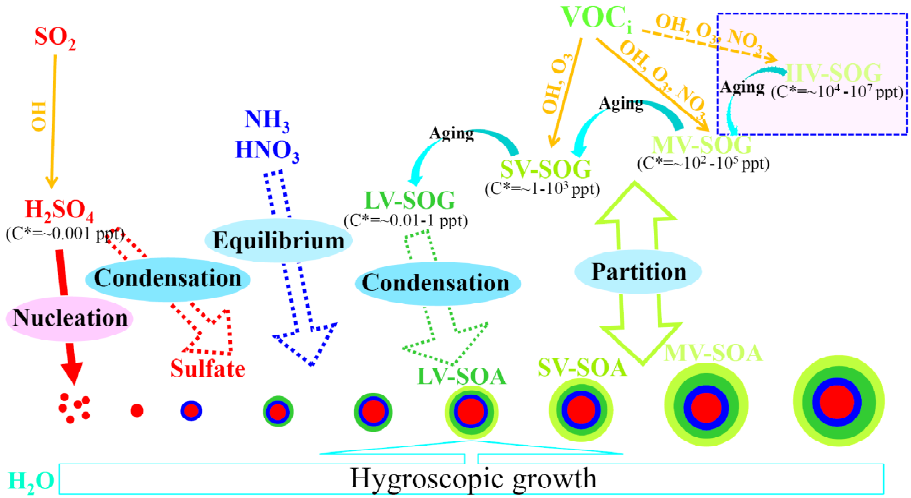

Fig. 2. Schematic illustration of particle formation and growth as well as oxidation aging processes in the atmosphere. See text for details.

ACPD
10, 19811–19844, 2010

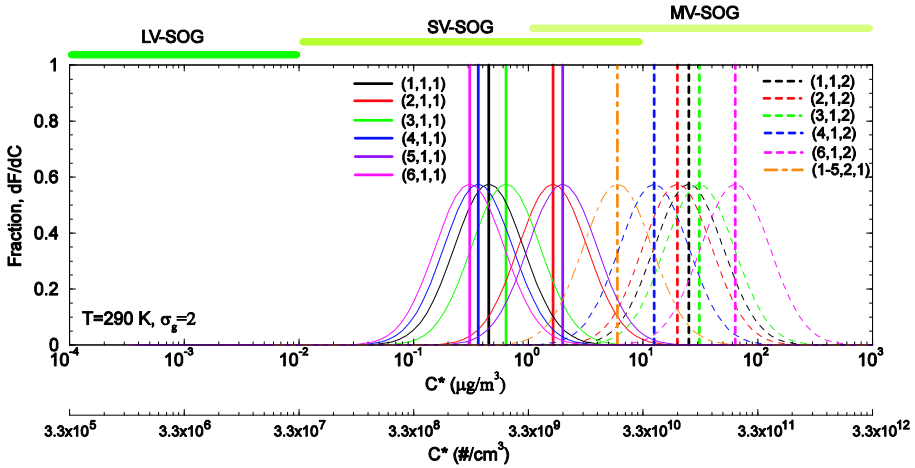

Fig. 3. Normalized distributions ($f_{SOG}(C^*)$, with geometric standard deviation σ_g=2) of $SOG_{i,j,k}$ at T=290 K. The vertical lines are the median C^*. Second x-axis of C^* in # cm^{-3} is calculated from C^* in μg m^{-3} based on molecular weight of 181 g mol^{-1}.

ACPD
10, 19811–19844, 2010

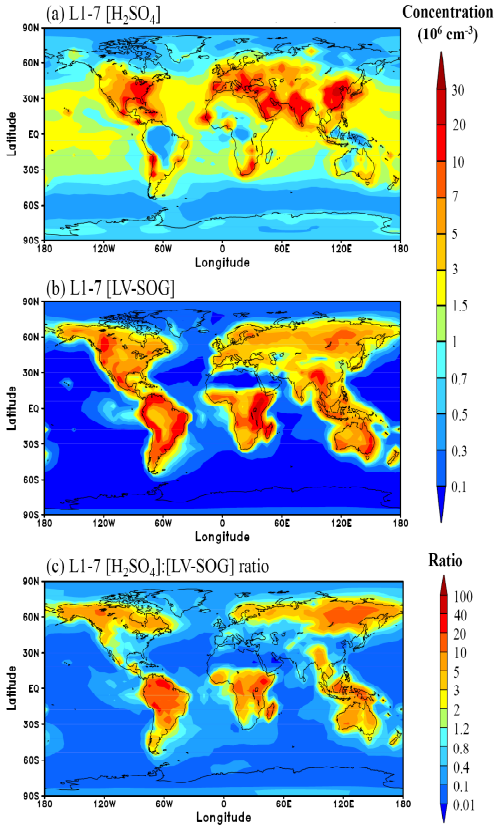

Fig. 4. Horizontal distributions (averaged over first seven model layers above Earth's surface: 0–1 km) of annual mean values of **(a)** H_2SO_4 gas concentration [H_2SO_4], **(b)** LV-SOG concentration [LV-SOG], and **(c)** ratio of [LV-SOG] to [H_2SO_4]. The simulation was carried out with GEOS-Chem+APM for year 2005 with a horizontal resolution of 4°×5° and 47 vertical layers up to 0.01 hpa (GEOS-5 meteorological fields).

ACPD
10, 19811–19844, 2010

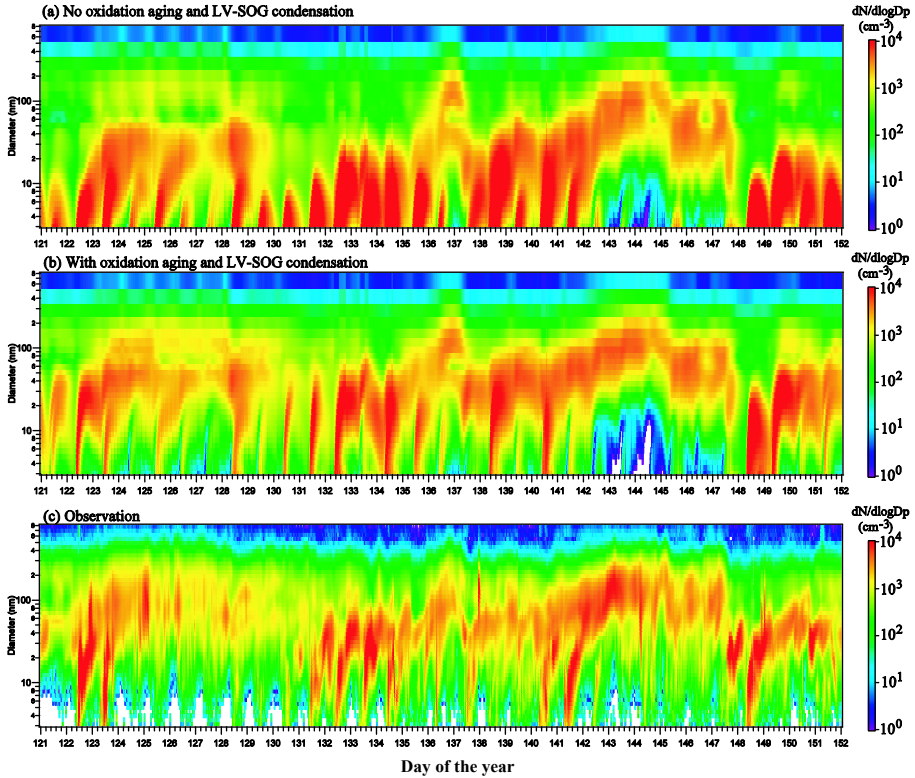

Fig. 5. A comparison of the simulated particle size distribution evolution based on **(a)** previous 2-product SOA formation model (i.e., no oxidation aging and explicit condensation of LV-SOG) and **(b)** extended SOA formation model described in Sect. 2, with **(c)** those observed in a boreal forest site (Hyytiälä, Finland) during May 2005. The simulations are the results for the surface layer. The observation data are from the CREATE Aerosol Database at NILU and Markku Kulmala is the PI of the data. Further information of the size distribution measurements can be found in Laakso et al. (2004) and Ehn et al. (2007).

ACPD
10, 19811–19844, 2010

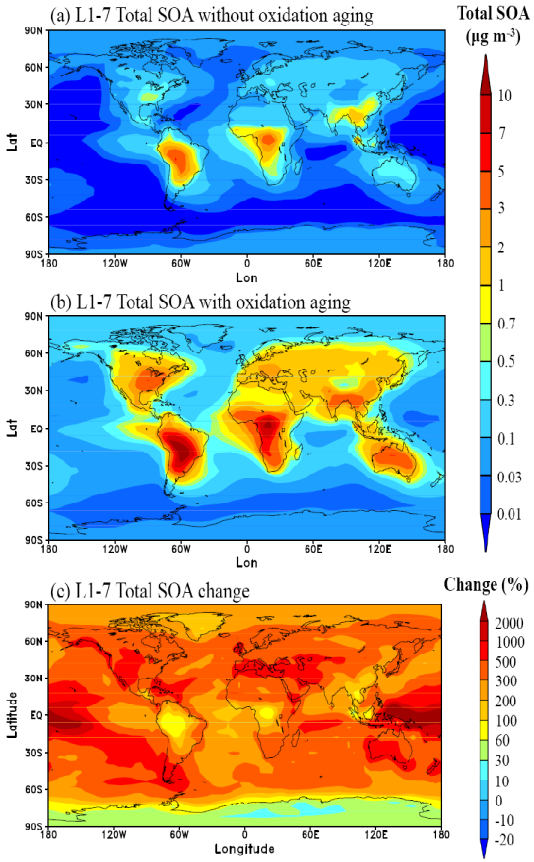

Fig. 6. Horizontal distributions of annual mean SOA mass concentrations in the boundary layer (0–1 km above surface) simulated **(a)** with original 2-product SOA formation model, **(b)** with the new extended SOA formation model described in this paper, and **(c)** percentage increase in SOA mass when SOG oxidation aging and LV-SOG condensation are considered.

ACPD
10, 19811–19844, 2010

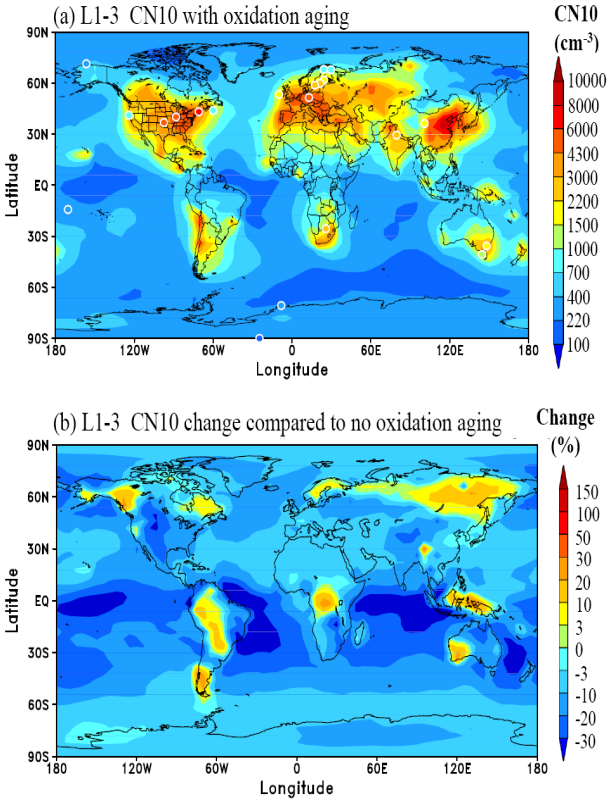

Fig. 7. **(a)** Horizontal distributions of annual mean number concentrations of condensation nuclei larger than 10 nm (CN10) in the lower boundary layer (0–0.4 km) simulated with new SOA formation model described in this paper. The observed annual or multiple year averaged CN10 values from 21 sites are also overlapped on the plots for comparison. See text for the sources of the data. **(b)** Percentage change in CN10 compared to the case without oxidation aging and LV-SOG condensation.

ACPD
10, 19811–19844, 2010

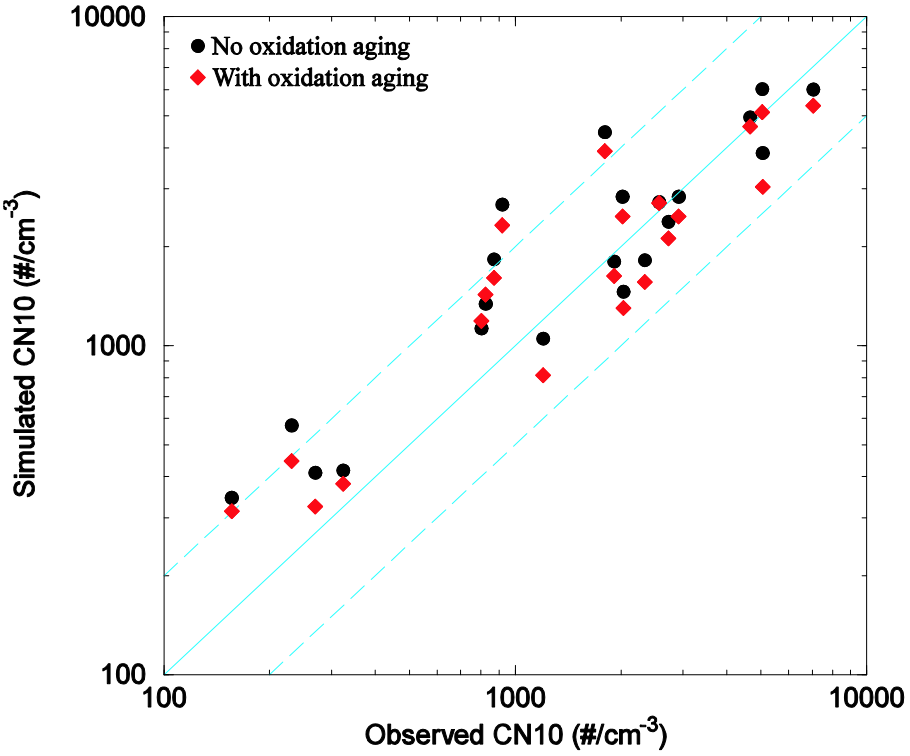

Fig. 8. Comparison of annually averaged number concentrations of CN10 observed at 21 sites shown in Fig. 7a with those simulated with and without LV-SOG condensation. The solid line shows a 1:1 ratio, and the dashed lines show ratios of 2:1 and 1:2.

ACPD
10, 19811–19844, 2010

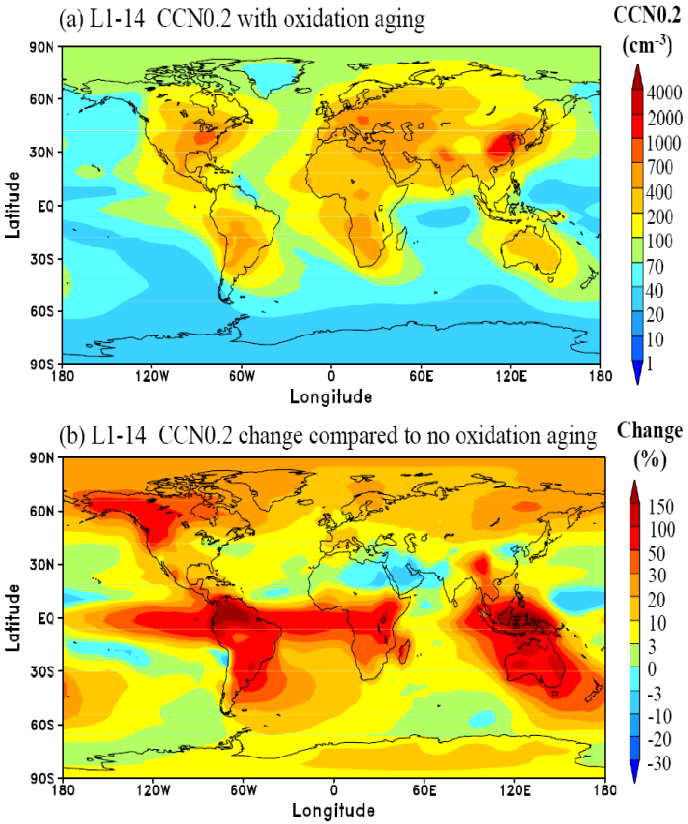

Fig. 9. (a) Horizontal distributions of annual mean number concentrations of cloud condensation nuclei at a water supersaturation ratio of 0.2% (CCN0.2) in the lower troposphere (0–2 km above surface) simulated with new SOA formation model described in this paper. **(b)** Percentage change in CCN0.2 compared to the case without oxidation aging and LV-SOG condensation.

ACPD
10, 19811–19844, 2010